SAPO-35 Molecular Sieve: Synthesis, Characterization, and Adsorbate Interactions of Cu(II) in CuH−SAPO-35

A. M. Prakash,[†] Martin Hartmann,[‡] and Larry Kevan*,[†]

Department of Chemistry, University of Houston, Houston, Texas 77204-5641, and Institut für Chemische Technologie I, Universität Stuttgart, 70550-Stuttgart, Germany

Received November 17, 1997. Revised Manuscript Received January 13, 1998

Synthesis of small-pore silicoaluminophosphate SAPO-35 (structurally analogous to the zeolite levyne) using hexamethyleneimine in aqueous and fluoride media is described for the first time. Pure, highly crystalline samples of SAPO-35 were obtained within a short reaction period of 24 h. Various factors affecting crystallinity and phase purity of SAPO-35 were studied. Samples were characterized by X-ray powder diffraction, ^{27}Al, ^{29}Si and ^{31}P solid state MAS NMR spectroscopy, FTIR spectroscopy, thermal analysis (TG and DTA), surface area measurement, electron microprobe analysis and scanning electron microscopy. SAPO-35 crystallizes with highly uniform rhombic crystals about 1 μm across. Two crystallographically distinct tetrahedral framework sites in SAPO-35 are shown from MAS NMR studies. ^{29}Si MAS NMR spectra show that silicon substitutes for framework phosphorus and generates large Bronsted acidity. The location of Cu(II) ions exchanged into H−SAPO-35 and their interaction with deuterated water, ammonia, methanol, and ethylene have been investigated by electron spin resonance (ESR) and electron spin−echo modulation (ESEM) techniques. Simulation parameters of the ^{31}P ESEM spectrum suggest that the hydrated Cu(II) complex, i.e., $Cu^{II}(H_2O)_6$, is located in the levyne cage. During dehydration some of the Cu(II) ions may migrate into double hexagonal prisms. Room-temperature adsorption of D_2O on CuH−SAPO-35 after dehydration at 723 K and subsequent O_2 treatment and evacuation at the same temperature (activation) forms a Cu(II)−aquo complex with axially symmetric ESR parameters ($g_{||} = 2.387$ and $A_{||} = 0.0151$ cm^{-1}). This complex is suggested to be $Cu^{II}(D_2O)_3$ based on ^{2}D ESEM data. Adsorption of ND_3 on activated CuH−SAPO-35 produces two $Cu^{II}(ND_3)_n$ complexes with axially symmetric ESR parameters. When CD_3OH is adsorbed on CuH−SAPO-35, the resultant Cu(II) complex with ESR parameters $g_{||} = 2.398$ and $A_{||} = 0.0142$ cm^{-1} contains one methanol molecule coordinating directly with the metal ion based on ^{2}D ESEM measurements. Adsorption of C_2D_4 on activated CuH−SAPO-35 gives two $Cu^{II}(C_2D_4)_n$ complexes based on ESR measurements.

Introduction

Silicon-substituted aluminophosphate molecular sieves (SAPOs) have been of considerable interest for producing materials with controlled acidity that may be used as catalysts in various reactions.[1] Small-pore molecular sieves such as SAPO-17 (erionite), SAPO-18 (chabazite-like), SAPO-34 (chabazite), and SAPO-35 (levyne) are particularly interesting materials since they show high activity and selectivity for methanol conversion to olefins (MTO).[2−4] SAPO-34 has shown the highest selectivity of about 90% toward lower olefins at 100% methanol conversion. Whereas the selectivity is attributed to the specific pore structures of these materials, the high activity is mainly due to the high Bronsted acidity of these materials arising out of isolated silicon substitution for framework phosphorus. Of the various SAPO structures, SAPO-35 is less studied although it is structurally analogous to the natural zeolite levyne. In the original UOP patent, only quinuclidine was identified as a suitable organic template for the crystallization of SAPO-35.[5] A high reaction temperature (473 K) and long crystallization period (144 h) are reported for obtaining pure SAPO-35. Later, Lohse et al.[6] reported that cyclohexylamine is a suitable template for the synthesis of SAPO-35. According to this route, SAPO-35 can be prepared only for a narrow range of silica concentrations in the gel. A levyne-like cobalt aluminophosphate, DAF-4, was designed using computer modeling of template geometry and pore structure; this was crystallized hydrothermally using 2-methylcyclohexylamine as a template.[7] Crystallization occurs at

[†] University of Houston.
[‡] Universität Stuttgart.

(1) Rabo, J. A.; Pellet, R. J.; Coughlin, P. K.; Shamshoun, E. S. In *Zeolites as Catalysts, Sorbents and Detergent Builders: Application and Innovations*; Karge, H. G., Weitkamp, J., Eds.; Elsevier: Amsterdam, 1989; Studies in Surface Science and Catalysis, Vol. 46, p 1.
(2) Inui, T.; Phatanasri, S.; Matsuda, H. *J. Chem. Soc., Chem. Commun.* **1990**, 205.
(3) Maxwell, I. E.; Naber, J. E. *Catal. Lett.* **1992**, *12*, 105.
(4) Wendelbo, R.; Akporiaye, D.; Andersen, A.; Dahl, I. M.; Mostad, H. B. *Appl. Catal. A: General* **1996**, *142*, L197.
(5) Lok, B. M.; Messina, C. A.; Patton, R. L.; Gajek, R. T.; Cannan. T. R.; Flanigen, E. M. U.S. Patent 4,440,871,1984.
(6) Lohse, U.; Vogt, F.; Richter-Mendau, J. *Cryst. Res. Technol.* **1993**, *28*, 1101.

S0897-4756(97)00752-7 CCC: $15.00
Published on Web 02/18/1998

473 K after a period of 168 h. The hexamethyleneimine template was previously identified as a suitable template for the synthesis of MCM-22 zeolite and for the extra-large-pore gallophosphate molecular sieve cloverite.[8,9] Very recently SAPO-35 molecular sieve has been prepared in a nonaqueous medium using hexamethyleneimine.[10] A temperature of 473 K for 384 h was reported for its crystallization. Here, we report an efficient synthesis route for SAPO-35 molecular sieve within a short reaction time (24 h) using hexamethyleneimine in both aqueous and fluoride media. The structural features of this material are studied by various characterization techniques and compared with previously synthesized SAPO-35 using other organic templates.

Cu-exchanged zeolites are highly efficient in oxidation reactions such as propylene to acrolein (CH_2=CHCHO) and in NO_x decomposition reactions.[11,12] Cu-exchanged SAPO molecular sieves are also thermostable catalysts for selective reduction of NO_x with hydrocarbons.[13] Of the various catalysts tested including SAPO-5, SAPO-11, SAPO-34, zeolite beta, USY, and ZSM-5, Cu−SAPO-34 was found to exhibit the highest activity for NO reduction at temperatures above 973 K. Levyne-like aluminophosphate molecular sieve has also been shown to exhibit interesting adsorptive and catalytic properties.[14] In the present paper we also report an ESR/ESEM study on the location and coordination geometry of Cu(II) in Cu(II)-exchanged SAPO-35 molecular sieve, Cu−SAPO-35.

Experimental Section

SAPO-35 was synthesized by hydrothermal crystallization under autogenous pressure without agitation. The starting materials were orthophosphoric acid (85%, Mallinckrodt), pseudoboehmite (Catapal-B, Vista), fumed silica (Sigma), and hexamethyleneimine (98%, Aldrich). Synthesis were carried out in 100 cm^3 stainless steel reactor lined with Teflon material. For pure, highly crystalline SAPO-35, the molar composition of the reaction mixture was 1.0 Al_2O_3:1.0 P_2O_5:(0.3−1.0) SiO_2:1.5 R:55 H_2O, where R is hexamethyleneimine. In a typical synthesis, 7.28 g of Catapal-B was slurried in 16 g of deionized water and stirred for 2 h. Then 11.53 g of phosphoric acid was diluted in 10 g of water and slowly added to the alumina slurry followed by the addition of 10 g of additional water. The mixture was stirred for another 3 h. To this, 0.90 g of silica was added followed by 10 g of water. After this was stirred for another 30 min, 7.53 g of hexamethyleneimine was added dropwise. The final mixture was stirred at room temperature for 24 h for aging. The pH of the final gel was about 5. Crystallization was done at 200 °C for 24 h. After crystallization the product was separated from the mother liquor, washed with water and dried at 373 K overnight. H−SAPO-35 was prepared by heating as-synthesized SAPO-35 slowly to 873 K in O_2 and maintaining it at this temperature for 12 h for removal of the organic template.

Table 1. Experimental Conditions for MAS NMR Measurements on SAPO-35

	^{27}Al	^{29}Si	^{31}P
resonance frequency/MHz	104.26	79.49	161.96
pulse duration/μs	0.61	CP	3.5
number of scans	2000	424	64
repetition time/s	0.5	10	30
reference	$Al(H_2O)_6^{3+}$	$Si(CH_3)_4$	H_3PO_4

CuH−SAPO-35, where Cu(II) ions exist in extraframework positions in the SAPO-35 structure was prepared by stirring 1 g of H−SAPO-35 with 20 mL of 1 mM $CuCl_2$ and 80 mL of H_2O at 330 K for 24 h. The ion-exchanged material was washed several times with water and dried at 330 K overnight.

X-ray powder diffraction (XRD) patterns were recorded on a Siemens D-5000 diffractometer using Cu Kα radiation. Solid-state MAS NMR studies were performed on a Bruker MSL400 spectrometer using standard 4 and 7 mm Bruker MAS probes. The rotors were spun at a frequency of 9.5 and 3.5 kHz, respectively. In the case of ^{31}P NMR, high-power proton decoupling was applied, while in the case of ^{29}Si NMR the cross-polarization technique (CP) was employed. The experimental conditions for the NMR measurements are summarized in Table 1. Differential thermal analysis (DTA) and thermogravimetric analysis (TG) were carried out on a Dupont 9900 thermal analyzer in air at a heating rate of 10 K min^{-1}. Scanning electron micrographic (SEM) observations and electron microprobe analysis were done on a JEOL JXA spectrometer. IR spectra were recorded on a Nicolet 740 FT-IR spectrophotometer. The surface area of the sample was measured on a Quantachrome Instrument using a single-point BET method.

For ESR and ESEM measurements, the CuH−SAPO-35 samples were loaded into 3 mm o.d. by 2 mm i.d. Suprasil quartz tubes and evacuated to a final pressure of 10^{-4} Torr at 295 K overnight. To study the behavior of the copper as a function of hydration, a sample was heated under vacuum from 295 to 673 K at regular intervals. For each interval, the temperature was raised slowly and the sample held at that temperature for 16 h. Then ESR spectra were measured at 77 K. To study the reduction behavior of CuH−SAPO-35, a sample was dehydrated at 673 K for 16 h and then contacted with 1 atm of O_2 at 673 K for 16 h followed by evacuation at the same temperature (activation). The activated sample was then contacted with 100 Torr of dry hydrogen at various temperatures for varying durations before ESR measurements. To prepare Cu(II) complexes with various adsorbates, activated samples were exposed to the room-temperature vapor pressure of D_2O (Aldrich Chemical), CD_3OH (Stohler Isotope Chemicals), 100 Torr of C_2D_4 (Cambridge Isotope Laboratories), and 90 Torr of ND_3 (Stohler Isotope Chemicals). These samples with adsorbates were sealed and kept at room temperature for 24 h before ESR and ESEM measurements.

ESR spectra were recorded with a Bruker ESP-300 X-band spectrometer at 77 K. The magnetic field was calibrated with a Varian E-500 gaussmeter. The microwave frequency was measured by a Hewlett-Packard HP 5342A frequency counter. ESEM spectra were measured at 4.5 K with a Bruker ESP 380 pulsed ESR spectrometer. Three pulse echoes were measured by using a $\pi/2-\tau-\pi/2-T-\pi/2$ pulse sequence as a function of time T to obtain a time domain spectrum. To minimize ^{27}Al, ^{27}Si, and ^{1}H modulations in measurements of phosphorus and deuterium modulations, the τ value was fixed accordingly depending on the magnetic field position. The phosphorus and deuterium modulations were analyzed by a spherical approximation for powder samples in terms of N

(7) Lewis, D. W.; Willock, D. J.; Catlow, C. R. A.; Thomas, J. M.; Hutchings, G. J. *Nature*, **1996**, *382*, 604
(8) Prakash, A. M.; Kevan, L. *J. Phys. Chem.* **1996**, *100*, 19587.
(9) Kessler, H.; Patanin, J.; Schott-Darie, C. In *Advanced Zeolite Science and Applications*; Jansen, J. C., Stocker, M., Karge, H. G., Weitkamp, J., Eds.; Elsevier: Amsterdam; 1994; Studies in Surface Science and Catalysis, Vol. 85, pp 75−113.
(10) Venkatathri, N.; Hegde, S. G.; Rajamohanan, P. R.; Sivasanker, S. *J. Chem. Soc., Faraday Trans.* **1997**, *93*, 3411.
(11) Ben Taarit, Y.; Che, M. In *Catalysis by Zeolites*; Imelik, B., Naccache, C., Ben Taarit, Y., Vedrine, C., Couduvier, G., Praliaud, H., Eds.; Elsevier: Amsterdam, 1980; Studies in Surface Science and Catalysis, Vol. 5, pp 167−193.
(12) Li, Y.; Hall, K. *J Catal.* **1991**,*129*, 202.
(13) Ishihara, T., Kagawa, M., Hadama, F., Takita, Y. In *Zeolites and Related Microporous Materials: State of the Art 1994*; Weitkamp, J., Karge, H. G., Pfeifer, H., Holderich, W., Eds.; Elsevier: Amsterdam, 1994; Studies in Surface Science and Catalysis, Vol. 84, pp 1493−1500.
(14) Barrett, P. A.; Jones, R. H.; Thomas, J. M.; Sanker, G.; Shannon, I. J.; Catlow, C. R. A. *Chem. Commun.* **1996**, 2001.

Table 2. Crystallization Parameters and Corresponding Products for AlPO and SAPO Materials in Syntheses Using Hexamethyleneimine (R)

	gel composition[a]							
expt	SiO_2	R	HF	aging, h	seed	temp, K	time, h	products (by XRD)
1		1.0				473	24	$AlPO_4$-16
2		1.0		24		473	24	$AlPO_4$-16
3		1.5				473	24	$AlPO_4$-5
4		1.5		24		473	24	$AlPO_4$-5 + unknown phase I
5		2.0				473	24	$AlPO_4$-5
6	0.1	1.5				473	24	SAPO-16 + SAPO-5
7	0.3	1.5				473	24	SAPO-16 + SAPO-35 + SAPO-5
8	0.3	2.0				473	24	SAPO-35 + unknown phase II
9	0.3	1.5		24		473	24	SAPO-35
10	0.6	1.5				473	24	SAPO-35
11	0.6	1.5		24		473	24	SAPO-35
12	0.3	1.5	1.0			473	24	SAPO-16 + SAPO-35
13	0.3	1.5	1.0	48		473	24	SAPO-35
14	0.3	1				473	24	SAPO-5 + SAPO-35
15	0.3	1.5				473	24	SAPO-35 + SAPO-5 + SAPO-16
16	0.3	1.5			yes	473	24	SAPO-35
17	0.3	1.5		24		448	24	SAPO-35 + SAPO-5
18	0.3	1.5		24		473	16	SAPO-35 + unknown phase III

[a] $1.0Al_2O_3$ $1.0P_2O_5$ $55H_2O$ plus the indicated mole ratios of SiO_2, R, and HF.

nuclei at distance R with an isotopic hyperfine coupling A_{iso}.[15] The best-fit simulation for an ESEM pattern is found by varying the parameters until the sum of the squared residuals is minimized.

Results

Although SAPO-35 can be crystallized in the presence of several organic templates, the use of hexamethyleneimine in aqueous and fluoride media is found to reduce the crystallization time significantly. Table 2 shows the various crystallization parameters employed in the present investigation and the corresponding products as determined by XRD. The concentration of silica, concentration of organic template and aging of the reaction gel have dramatic influences for the final product. In the absence of any silica in the gel, the product is either $AlPO_4$-16 or $AlPO_4$-5 depending on the concentration of the template. At lower template concentration $AlPO_4$-16 crystallizes in good yield, and at higher template concentration $AlPO_4$-5 crystallizes preferentially. When the concentration of silica is low (<0.2 mol), SAPO-16 is predominantly obtained with a minor phase of SAPO-5. At higher silica concentration (>0.2 mol) SAPO-35 and SAPO-5 are also competing phases. However, crystallization of pure SAPO-35 can be obtained either by aging the gel at room temperature for 24 h or by further increasing the silica concentration. The presence of fluoride ions in the synthesis gel has no significant effect on the crystallization of SAPO-35. In fluoride medium, also pure SAPO-35 can be crystallized from gels having a wide range of silica concentrations (0.03−1.0 mol). Lowering the crystallization temperature and the time of a synthesis batch that would otherwise yield SAPO-35 results in minor additional phases of SAPO-5 and an unknown structure type, respectively.

Typical X-ray diffraction patterns for as-synthesized SAPO-35 prepared in both aqueous and fluoride media are presented in Figure 1. The interplanar spacing (d values) and the corresponding intensity of SAPO-35

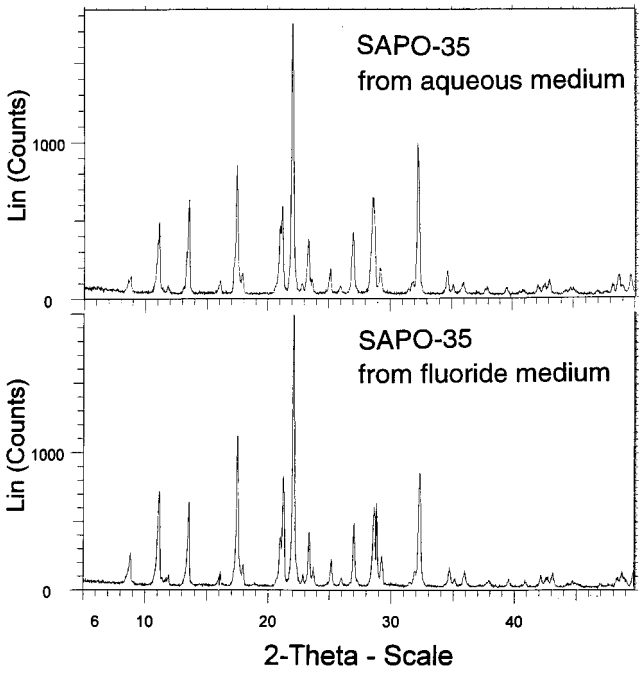

Figure 1. X-ray powder diffraction patterns for as-synthesized SAPO-35 prepared from aqueous (top) and fluoride (bottom) media using hexamethyleneimine.

synthesized using hexamethyleneimine match well with the corresponding values reported for SAPO-35 prepared with other templates.[5,6] The SAPO-35 crystals synthesized in aqueous medium belong to a hexagonal system with lattice parameters $a = 13.239$ Å, $b = 13.239$ Å, $c = 22.646$ Å, $\gamma = 120°$, and $V = 3437.5$ Å^3. Formation of pure, highly crystalline SAPO-35 is inferred from the XRD studies. The XRD patterns for the calcined sample are essentially the same, although slight reductions in intensity of some lines are observed. A highly crystalline sample of SAPO-35 (expt 9 in Table 2) was used for further characterization of this material and also for preparing CuH−SAPO-35.

Morphological features of as-synthesized SAPO-35 were observed by scanning electron microscopy. Figure 2 shows a SEM micrograph of SAPO-35 crystals that show cubelike rhombohedra. Highly uniform crystals

(15) Kevan, L. In *Time Domain Electron Spin Resonance*; Kevan, L., Schwartz, R. N., Eds.; Wiley: New York, 1979; Chapter 8.

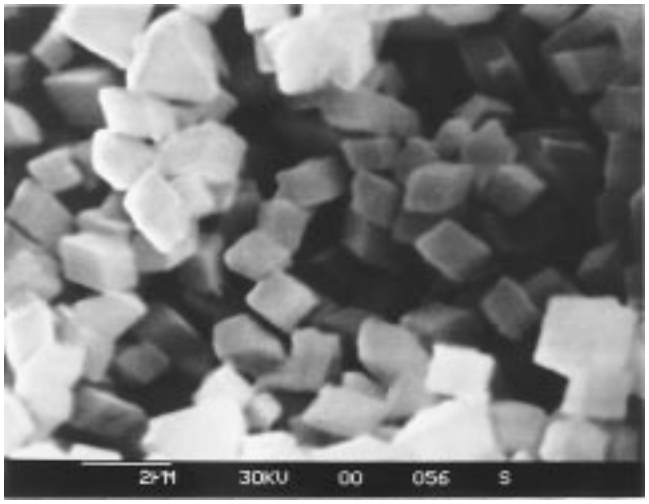

Figure 2. Scanning electron micrograph of SAPO-35 prepared from an aqueous medium using hexamethyleneimine as template.

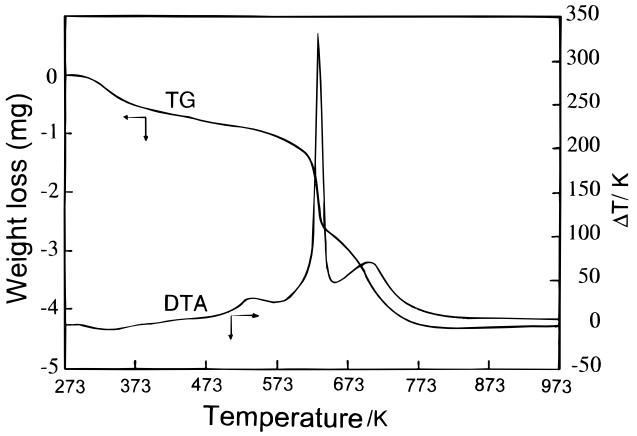

Figure 3. Thermogravimetric and differential thermal analysis profiles for as-synthesized SAPO-35.

about 1 μm across are observed. The morphological features of SAPO-35 synthesized in aqueous medium using hexamethyleneimine are different from those reported in nonaqueous media using the same template or in a system containing cyclohexylamine.[6,10] Using hexamethyleneimine in nonaqueous media or cyclohexylamine in aqueous media, spherical bundles of platelets with a spheroid size of 25−35 μm are reported. The present morphology is different from the natural zeolite levyne, which commonly forms thin, hexagonal platelets, 2−5 μm across, composed of twinned rhombohedra.[16]

IR spectra of SAPO-35 are essentially similar to those reported earlier for SAPO-35.[10] Figure 3 presents the TG and DTA profiles of SAPO-35. A low-temperature endotherm ascribable to the desorption of water and three high-temperature exotherms attributable to the desorption and decomposition of the organic template are the characteristic features. The weight loss observed between 250 and 473 K is about 3% and that between 473 and 873 K is about 15% for the amount of water and organic molecules, respectively. The chemical composition of this material determined by micro-

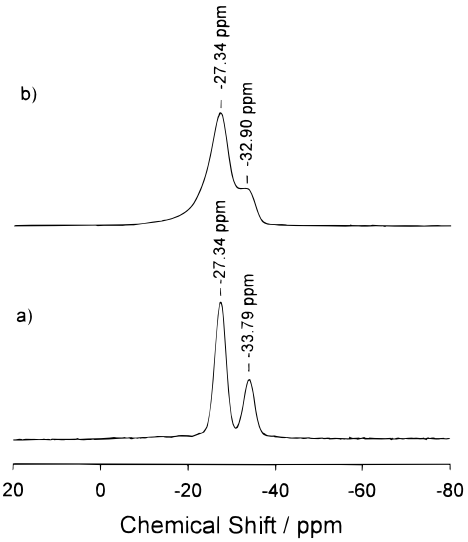

Figure 4. ^{31}P MAS NMR spectra of (a) as-synthesized and (b) calcined SAPO-35 molecular sieves.

probe analysis and TA data is 0.11R $(Si_{0.1}Al_{0.50}P_{0.40})O_2$. The unit-cell composition can then be estimated by assuming 54 T atoms/unit cell as 5.94R $(Si_{5.4}Al_{27}P_{21.6})$-$O_{108}$. The Si/Al ratio is 0.2, which is the same as the Si/Al ratio observed for SAPO-35 prepared in the presence of quinuclidine and cyclohexylamine. There are about six templating molecules occluded in each unit cell of SAPO-35 or one molecule/levyne cage. A similar value has been reported for SAPO-35 synthesized from nonaqueous media using hexamethyleneimine and from aqueous media using cyclohexylamine.[6,10] The surface area measured for SAPO-35 is 230 m^2/g. This value is higher than the values observed for large-pore SAPO-5 (214 m^2/g) and medium-pore SAPO-11 (123 m^2/g). The large levyne cage in the SAPO-35 structure may be responsible for the higher surface area of this material in comparison with one-dimensional channel-type materials such as SAPO-5 and SAPO-11.

^{27}Al, ^{29}Si, and ^{31}P MAS NMR spectra of SAPO-35 were recorded to ascertain the environment of these ions in the structural framework. The ^{31}P MAS NMR spectra of hydrated, as-synthesized SAPO-35 (Figure 4a) exhibits two lines at −27.34 and −33.79 ppm with an intensity ratio close to 2:1, characteristic of tetrahedral phosphorus in the framework. Upon calcination (Figure 4b) the lines broaden considerably, but two lines at −27.34 and −32.90 ppm are still distinguishable. The major ^{27}Al NMR line at 35.0 ppm in as-synthesized SAPO-35 (Figure 5a) is in agreement with tetrahedral aluminum in a silicoaluminophosphate framework. The broad shoulder at lower frequency indicates some higher coordinated aluminum. In the spectrum of a calcined sample two lines at 33.9 and −11.7 ppm can be detected. The line at −11.7 ppm is probably caused by aluminum atoms with octahedral oxygen coordination.[17] Two ^{29}Si NMR signals at −89.1 and −94.9 ppm are observed in as-synthesized SAPO-35 (Figure 6a). Due to the nature of the CP experiment no information on the intensity ratio is obtained. Upon calcination, the signals broaden and overlap.

(16) Tschernich, R. W. *Zeolites of the World*; Geoscience Press: Phoenix, 1992; p 295.

(17) Mueller, D.; Grunze, I.; Hallas, E.; Ladwig, G. *Z. Anorg. Allg. Chem.* **1983**, *500*, 80.

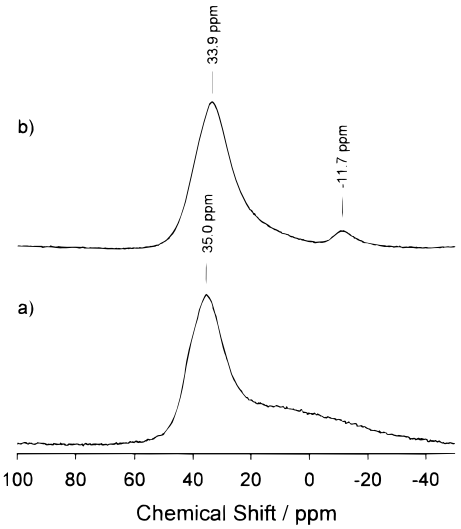

Figure 5. ^{27}Al MAS NMR spectra of (a) as-synthesized and (b) calcined SAPO-35 molecular sieves.

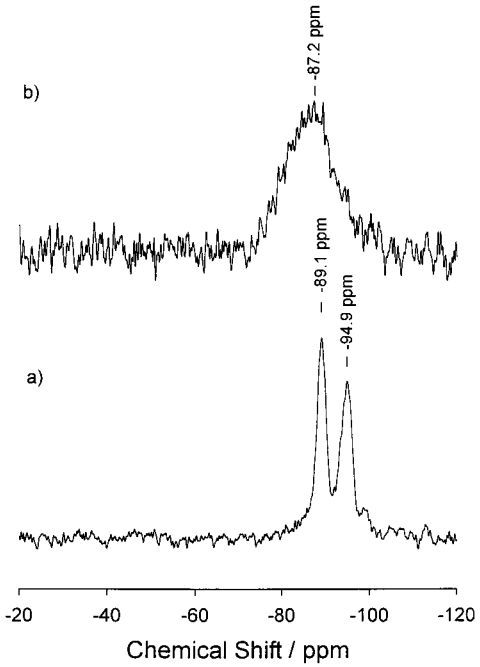

Figure 6. ^{29}Si CP MAS NMR spectra of (a) as-synthesized and (b) calcined SAPO-35 molecular sieves.

The ESR spectrum of hydrated CuH−SAPO-35 is shown in Figure 7. The spectral parameters are $g_{\|} = 2.364$, $A_{\|} = 0.0149$ cm^{-1}, and $g_{\perp} = 2.078$ and correspond to a hexaaquocopper(II) complex.[18] Evacuation at higher temperatures starts removing water ligands and the corresponding ESR spectrum shows two Cu(II) species (Figure 7b). Species A and a new species B with $g_{\|} = 2.311$, $A_{\|} = 0.0177$ cm^{-1} are observed. Upon dehydration of the sample at 673 K, species A and B reduce their intensity with the concomitant formation of an isotropic signal at $g = 2.003$. It has been reported in Cu-exchanged mordenite that dehydration at temperatures above 573 K causes a reduction by half of the ESR signal of Cu(II).[19] Similar behavior is also observed in Cu-exchanged SAPO-17.[20] Reduction of Cu(II) to Cu(I) by

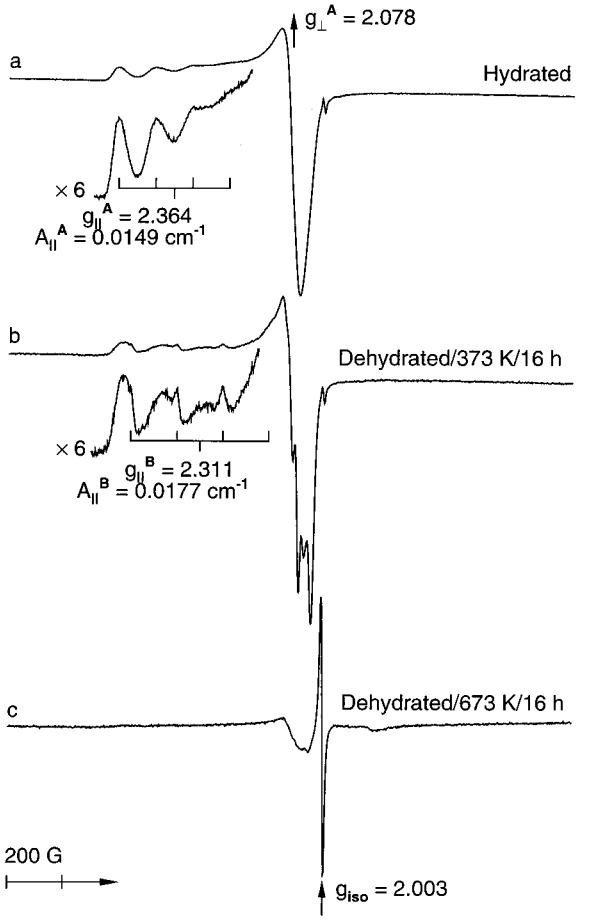

Figure 7. ESR spectra at 77 K of CuH−SAPO-35 (a) hydrated, (b) after dehydration at 373 K for 16 h, and (c) after dehydration at 673 K for 16 h.

residual water has been suggested for this intensity decrease. During the process, water decomposes into oxygen and hydrogen. The decomposition of water has been observed with other transition-metal-exchanged zeolites also.

As shown in Figure 8a, when a previously dehydrated sample is treated with O_2 at 673 for 16 h, the corresponding ESR spectrum regains its intensity with the formation of two Cu(II) species D and E. The ESR parameters of these two species are $g_{\|} = 2.342$; $A_{\|} = 0.0143$ cm^{-1} and $g_{\|} = 2.310$, $A_{\|} = 0.0168$ cm^{-1}, respectively. After evacuation of the oxygen at room temperature and treatment with H_2 at 295 K, an ESR spectrum similar to that observed for an activated sample is observed (Figure 8b). However, when this hydrogen-treated sample is heated to higher temperatures, species D reduces its intensity significantly. At 673 K species D disappears completely while species E retains its intensity (Figure 8c). The disappearance of species D is attributed to the reduction of Cu(II) ions to Cu (I) in the presence of hydrogen.

ESR spectra for CuH−SAPO-35 after adsorbing D_2O, ND_3, C_2D_4, and CD_3OH are given in Figure 9. When D_2O is adsorbed on an activated sample, an ESR signal similar to that observed for a hydrated sample is obtained (Figure 9a). The ESR parameters of Cu(II)

(18) Herman, R. G. *Inorg. Chem.* **1979**, *18*, 995.

(19) Kasai, P. H.; Bishop, Jr., R. J. *J. Phys. Chem.* **1977**, *81*, 1527.
(20) Prakash, A. M.; Kevan, L *Langmuir* **1997**, *13*, 5341.

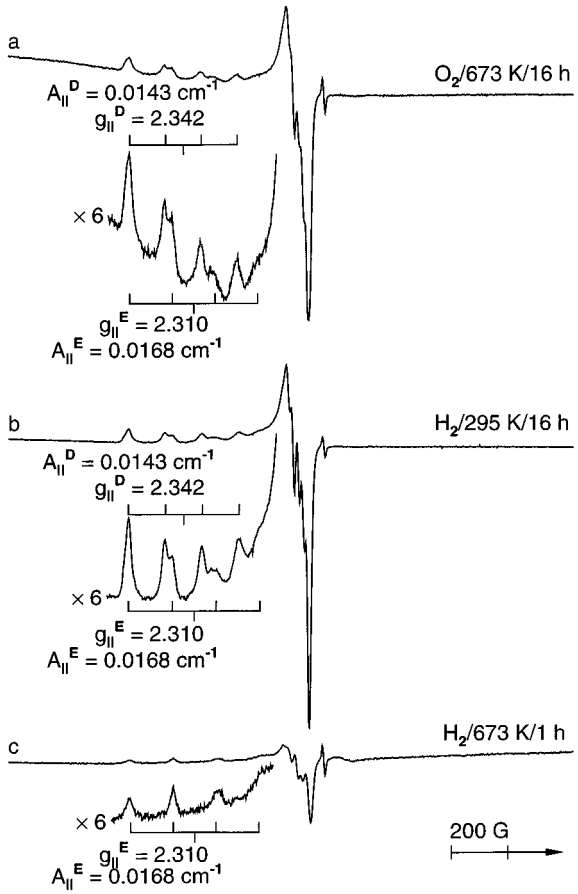

Figure 8. ESR spectra at 77 K of CuH−SAPO-35 (a) after O_2 treatment of a dehydrated sample at 673 K for 16 h and subsequent evacuation, (b) after H_2 treatment of an activated sample at 295 K for 16 h, and (c) after H_2 treatment of an activated sample at 673 K for 1 h.

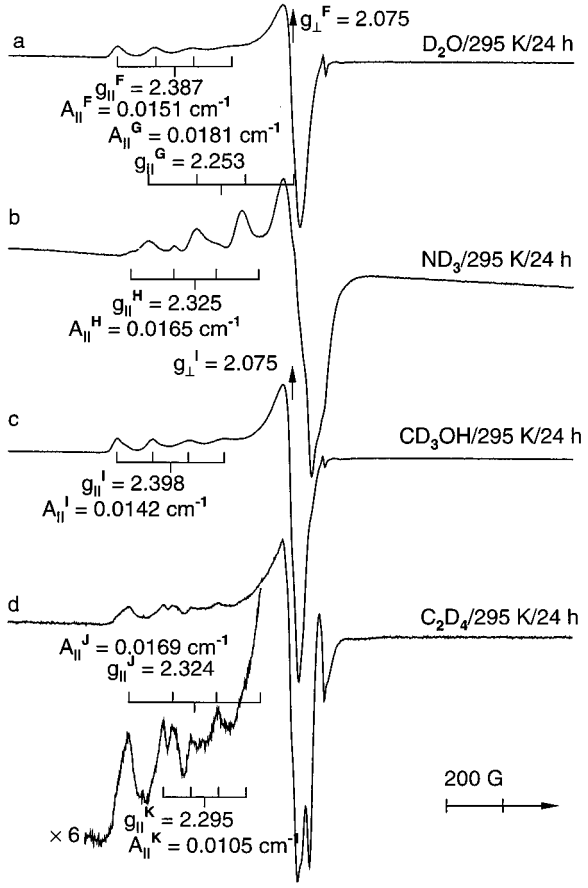

Figure 9. ESR spectra at 77 K of CuH−SAPO-35 (a) after D_2O adsorption on an activated sample at 295 K for 24 h, (b) after ND_3 adsorption on an activated sample at 295 K for 24 h, (c) after CD_3OH adsorption on an activated sample at 295 K for 24 h, and (d) after C_2D_4 adsorption on an activated sample at 295 K for 24 h.

species F observed after D_2O adsorption are $g_{||} = 2.387$ and $A_{||} = 0.0151$ cm^{-1}, which are slightly different from those of species A in an originally hydrated sample. When ND_3 is adsorbed at 295 K on an activated sample of CuH−SAPO-35, two new Cu(II) species G and H with axially symmetric ESR parameters ($g_{||} = 2.253$ and $A_{||} = 0.0181$ cm^{-1} for species G and $g_{||} = 2.325$ and $A_{||} = 0.0165$ cm^{-1} for H) are observed (Figure 9b). When CD_3OH is adsorbed on an activated sample of CuH−SAPO-35, a new Cu(II) species I with axial ESR parameters ($g_{||} = 2.398$, $A_{||} = 0.0142$ cm^{-1} and $g_\perp = 2.075$) is observed (Figure 9c). When deuterated ethylene is adsorbed on activated CuH−SAPO-35, two new Cu(II) species J and K with axially symmetric ESR parameters are observed (Figure 9d). The ESR parameters are $g_{||} = 2.324$ and $A_{||} = 0.0169$ cm^{-1} for species J and $g_{||} = 2.295$ and $A_{||} = 0.0105$ cm^{-1} for species K. No noticeable change in the ESR intensities of the various Cu(II) species is observed even after annealing the sample at room temperature for several days. The ESR parameters of the various Cu(II) species are summarized in Table 3.

Table 3. ESR Parameters at 77 K for Cu(II) Ions in CuH−SAPO-35 after Various Treatments

treatment	species	assignment	$g_{||}$	$A_{||}$ (cm^{-1})	$g_\perp$
fresh	A	$Cu^{II}(H_2O)_6$	2.364	0.0149	2.078
dehydrated	D	Cu^{II}	2.342	0.0143	nr[a]
	E	Cu^{II}	2.310	0.0168	nr[a]
+D_2O	F	$Cu^{II}(D_2O)_3$	2.387	0.0151	2.075
+ND_3	G	$Cu^{II}(ND_3)_n$	2.253	0.0181	nr[a]
	H	$Cu^{II}(ND_3)_n$	2.325	0.0165	nr[a]
+CD_3OH	I	$Cu^{II}(CD_3OH)_1$	2.398	0.0142	2.075
+C_2D_4	J	$Cu^{II}(C_2D_4)_n$	2.324	0.0169	nr[a]
	K	$Cu^{II}(C_2D_4)_n$	2.295	0.0105	nr[a]

[a] nr = not resolved.

Three-pulse ESEM spectra were recorded at magnetic fields corresponding to $g_\perp$ of various Cu(II) species. ^{31}P ($I = 1/2$, $\upsilon = 6.038$ MHz at 3500 G, 100% abundance), ^1H ($I = 1/2$, $\upsilon = 14.902$, 99.98%) and ^2D($I = 1$, $\upsilon = 2.288$ MHz, 99.8%) nuclei were investigated for spin−echo modulation. For a particular nucleus, the delay between the first and second pulses (τ) was selected so as to minimize modulation from other magnetic nuclei present in the system. Figure 10 shows the ^{31}P ESEM spectrum of hydrated and activated CuH−SAPO-35. Although a strong echo is observed in these samples, the modulation due to ^{31}P nuclei is weak. In a hydrated sample an approximate simulation of the spectrum shows two nearest neighbor phosphorus atoms at a distance of about 4.0 Å. The hydrated nature of the Cu(II) species in this sample is also evidenced by the strong ^1H modulation observed. As shown in Figure 10b, compared to a hydrated sample, a relatively strong ^{31}P modulation is observed for an activated sample, indicating a shorter distance between Cu(II) and the phosphorus nuclei. Since the spectrum contains contributions

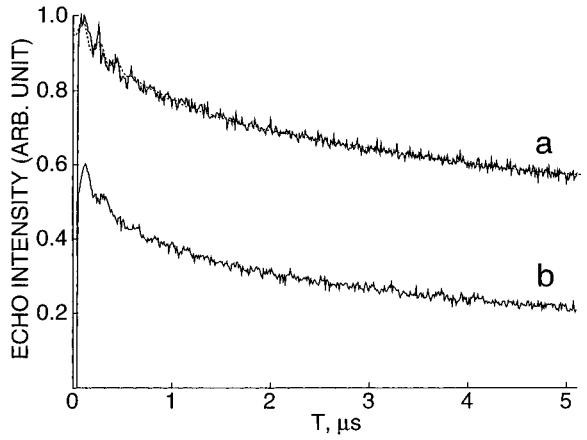

Figure 10. (a) Experimental (—) and simulated (···) three pulse ^{31}P ESEM spectra of hydrated CuH−SAPO-35 at the magnetic field corresponding to $g_\perp$ of species A and (b) experimental three pulse ^{31}P ESEM spectra of activated CuH−SAPO-35 at the magnetic field corresponding to $g_\perp$ of species D and E.

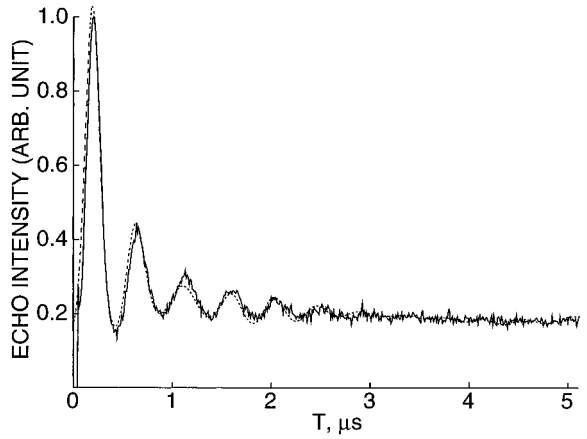

Figure 11. Experimental (—) and simulated (···) three-pulse ^{2}D ESEM spectra of CuH−SAPO-35 after D_2O adsorption. The spectrum was recorded at the magnetic field corresponding to $g_\perp$ of species F.

from both Cu(II) species D and E, simulation of the spectrum was not attempted.

Figure 11 shows the experimental and simulated ^{2}D ESEM spectrum of CuH−SAPO-35 with adsorbed D_2O. The magnetic field was set at $g_\perp$ of species F (Figure 9a). Simulation of the spectrum gives six deuterium nuclei at a distance of 2.8 Å and another two nuclei at a distance of 4.6 Å. These values are consistent with three D_2O molecules coordinating directly with Cu(II) and one D_2O molecule interacting from a farther distance. The experimental and simulated ^{2}D ESEM spectrum of CuH−SAPO-35 after adsorbing CD_3OH is shown in Figure 12. The field was set at $g_\perp$ of species I (Figure 9c). The spectrum can be simulated by three deuterium nuclei at 3.4 Å and three nuclei at 5.1 Å. These parameters can be rationalized in terms of one directly coordinated methanol and another indirectly interacting methanol at a farther distance. Although strong deuterium modulations are observed in CuH−SAPO-35 samples containing ND_3 and C_2D_4, no quantitative analyses were attempted due to the unknown contributions of the multiple Cu(II) species in these samples.

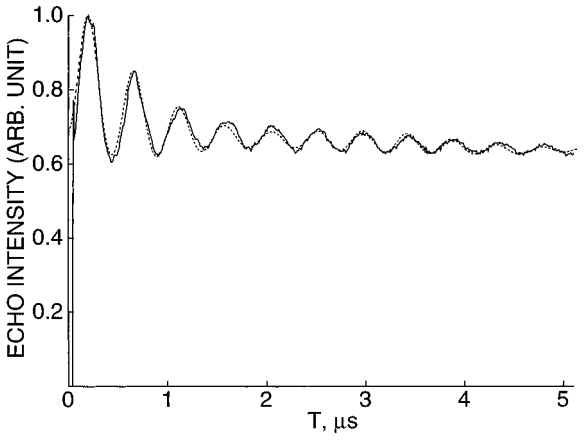

Figure 12. Experimental (—) and simulated (···) three-pulse ^{2}D ESEM spectra of CuH−SAPO-35 after CD_3OH adsorption. The spectrum was recorded at the magnetic field corresponding to $g_\perp$ of species I.

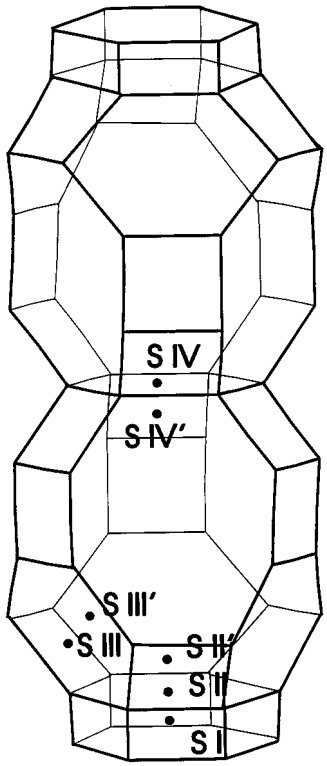

Figure 13. Polyhedral cages found in SAPO-35 molecular sieve. Also shown are possible cation positions. See text for description of the cation positions.

Discussion

SAPO-35 is a small pore molecular sieve with eight-membered ring pore openings. As shown in Figure 13 the polyhedral cages observed in SAPO-35 are hexagonal prisms and levyne cages. The levyne cages are connected through six-rings and double six-rings. These cages are accessible through eight-membered windows of dimension 3.6 × 4.8 Å. There are two crystallographically distinct T sites in the framework, one in a double six-ring and the other in a single six-ring. The distribution of these two sites are in the ratio 2:1. The observed two resonances in the ^{31}P NMR spectrum with an intensity ratio 2:1 corresponds to phosphorus atoms at these two sites. The chemical composition of SAPO-35 suggests that Si atoms substitute for framework

phosphorus sites. Consequently, the two signals observed in ^{29}Si NMR spectrum of as-synthesized SAPO-35 are assigned to Si substitution for phosphorus at these two crystallographically independent sites. The ^{27}Al MAS NMR spectrum of aluminophosphate molecular sieve is generally consistent with tetrahedral aluminum modified by second-order quadrupolar coupling and interaction with entrapped template or water molecules. Crystallographically independent sites are normally not resolved in ^{27}Al MAS NMR spectra but can be distinguished by the application of double rotation ^{27}Al NMR. The ^{27}Al MAS NMR spectra of SAPO-35 show a single resonance near 34 ppm charactersitic of tetrahedral aluminum in the framework. The asymmetric nature of this line supports the presence of two crystallographically different tetrahedral sites in the framework of SAPO-35, which is confirmed by the ^{31}P and ^{29}Si MAS NMR data in Figures 4 and 6.

In SAPO-35, several cationic sites can be identified. On the basis of the structural model of SAPO-35 and by analogy with the cation positions in the analogous zeolite levyne,[21] the possible cation sites in SAPO-35 are shown in Figure 13. Site S I is the center of a hexagonal prism. Site S II is the center of a six-ring window joining a levyne cage and a hexagonal prism. Site S II′ is site S II displaced toward the center of a levyne cage. Site S III is the center of a six-ring window of a levyne cage. Site S III′ is site S III displaced toward the center of a levyne cage. Site S IV is the center of a six-ring joining two levyne cages. Site S VI′ is S IV displaced toward the center of either levyne cage. In natural zeolites, cations are found to occupy selected sites depending on the cation types.[21] In natural zeolite levyne, Na^+ and K^+ ions normally occupy sites S III′, S IV, and S IV′, while Ca^{2+} ions occupy site S II′.

The ESR parameters of Cu(II) species observed in hydrated CuH−SAPO-35 have been previously assigned to a hexacoordinated $Cu^{II}(H_2O)_6^{2+}$ complex.[18] This assignment is supported by both ^{31}P and ^{1}H ESEM spectra observed here. There is no direct interaction between framework oxygens and the Cu(II) ions as suggested by the 4.0 Å distance observed between Cu(II) and the nearest-neighbor P nuclei. A direct interaction between framework oxygen and Cu(II) ions would mean a nearest-neighbor distance to P of about 3.2 Å. Substitution of Si for P in the framework of SAPO-35 generates a net framework negative charge which is balanced by protonated templating species in the as-synthesized form and by H^+ in the calcined form. During ion exchange with Cu^{2+}, some of these H^+ ions will be replaced by the $Cu(H_2O)_6^{2+}$ ions. The water ligated Cu ions take position in the vicinity of a Si ion within a levyne cage. Due to size constraints offered by the six-ring window, it is unlikely that the hydrated copper ions exchange into positions within a hexagonal prism or are at the center of six-ring windows. However, there is no size constraint for $Cu(H_2O)_6^{2+}$ ions to occupy positions at the center of eight-ring windows or near six-ring windows within the levyne cage. From the chemical composition of SAPO-35, there are 3−4 P atoms in an eight-ring window and 2−3 P atoms in a six-ring window. Thus the observed ^{31}P ESEM simulation parameters of 2 P atoms at 4 Å can then be rationalized in terms of an aquo-ligated Cu(II) complex situated within a levyne cage near the center of a six-ring window in which one of the P sites is occupied by Si. The Cu(II) complex may interact with the framework by interaction between hydrogen of its water ligands and framework oxygen.

During dehydration of CuH−SAPO-35, the $Cu^{II}(H_2O)_6^{2+}$ complex loses some of its water ligands to form new complexes as evidenced by the two Cu(II) species A and B observed. A second effect of dehydration is the substantial decrease in the intensity of the Cu(II) species. This effect is more prominant at temperatures above 573 K. This loss in intensity of Cu(II) species is attributed to reduction of Cu(II) to Cu(I) by residual water with water decomposition. The following reaction mechanism has been proposed[19] for the reduction of Cu(II) to Cu(I) by water where M represents the molecular sieve:

$$[2\mathrm{Cu(II)}, n\mathrm{H_2O}]\mathrm{M} \rightarrow [2\mathrm{Cu(II)}, 2\mathrm{H^+}, 2\mathrm{OH^-}]\mathrm{M} \rightarrow [2\mathrm{Cu(I)}, 2\mathrm{H^+}]\mathrm{M} + \mathrm{H_2O} + {}^1/_2\mathrm{O_2}\uparrow$$

When a previously dehydrated sample of CuH−SAPO-35 is treated with O_2 at high temperature, the ESR spectrum regains its original intensity with the formation of two Cu(II) species, D and E. A possible explanation is the oxidation of Cu(I) to Cu(II) and migration of some of the Cu(II) to new locations within the SAPO-35 structure. Migration of metal ions from large channels and cages to smaller ones during dehydration is observed in several zeolites and other molecular sieves.[22] In zeolites having low Si/Al ratios, the high negative charge density inside small cavities and channels provides the main driving force for the migration of transition-metal ions from larger channels or supercages to smaller ones. A typical example of this phenomenon is in transition metal exchanged zeolites X and Y, where the metal ions located initially within a large supercage migrate to a smaller sodalite cage during dehydration.[22] Similar effects are observed in metal ion exchanged SAPO-5 and SAPO-11 molecular sieves. The metal ions located initially in the main 12-ring or 10-ring channel migrate to 6-ring channels during dehydration.[23] In SAPO-17 some of the metal ions initially located within a large erionite cage migrate to smaller cancrinite cages and hexagonal prisms during dehydration.[20] The main driving force for cation migrations in SAPO materials is probably the negative framework charge generated by the substitution of Si for framework P sites. According to chemical analysis one unit cell of SAPO-35 contains a maximum of six Si substituting for P sites or one per each levyne cage. The specific location of Si ions within a unit cell may then influence the migration of Cu(II) ions during dehydration. In activated CuH−SAPO-35, ^{31}P ESEM is not effective in identifying the location of the Cu(II) species because of the superposition of the ESR spectra of species D and E. Possible migration of Cu(II) ions in SAPO-35 is from a larger levyne cage to a smaller hexagonal prism. Structurally

(21) Mortier, W. J. *Compilation of Extra-framework Sites in Zeolites*; Structure Commission of the International Zeolite Association; Butterworth: Surrey, 1982; p 39.

(22) Sachtler, W. H. M.; Zhang, Z. *Adv. Catal.* **1993**, *39*, 129.
(23) Lee, C. W.; Chen, X.; Kevan, L. *Catal. Lett.* **1992**, *15*, 75.

similar sites have been suggested for the migration of Cu(II) ions after dehydration in several other Cu-exchanged zeolites and SAPO molecular sieves.[20,22,23]

The effect of hydrogen at high temperature on an activated sample is to remove Cu(II) species D and to retain Cu(II) species E. This suggests that species D is located at sites easily accessible to hydrogen which is then reduced to Cu(I). Cation sites S II′, S III′, and S IV′ within a levyne cage are more easily accessible to hydrogen than is site S I inside a hexagonal prism. Thus, we assign species D to Cu(II) ions located inside a levyne cage and species E to Cu(II) ions located inside a hexagonal prism.

Adsorption of D_2O on an activated sample generates an ESR spectrum similar to that observed for a hydrated sample. The parameters are characteristic of distorted octahedral Cu(II).[24] ^{2}D ESEM shows three D_2O molecules directly coordinated to Cu(II). A possible geometry for this complex is Cu(II) coordinated to three oxygens of D_2O and three oxygens from the framework. One more D_2O molecule interacts indirectly at a farther distance from the opposite side of the six-ring window.

Four different Cu(II) species corresponding to different degrees of water coordination have been identified in zeolites and other molecular sieves.[25] Depending on the pretreatment and the type of cocations present, Cu(II) complexes such as $Cu^{II}(O_z)_3(D_2O)_3$ (distorted octahedral), $Cu^{II}(O_z)_3(D_2O)_2$ (trigonal bypyramidal), and $(Cu^{II}(O_z)_3(D_2O)_1$ (distorted tetrahedral) have been observed in Cu-exchanged zeolite A. Here O_z represents framework oxygen. In Cu-exchanged faujasite type X zeolite, trigonal $Cu^{II}(O_z)(D_2O)_0$, trigonal-bipyramidal and distorted octahedral Cu(II) complexes have been observed. Similar to the present case of CuH−SAPO-35, in CuH−SAPO-17 (eronite structure) and CuH−SAPO-34 (chabazite structure) Cu(II) directly coordinates with three water molecules forming a distorted octahedral complex after D_2O adsorption.[20,26] Note that all these small-pore materials (SAPO-17, SAPO-34, and SAPO-35) are characterized by large cages and thus provide no spatial constraints to form trigonal-bypyramidal or distorted octahedral complexes.

When ND_3 is adsorbed on activated CuH−SAPO-35 two Cu(II) species G and H are observed. These two species probably differ in their location and coordination with ND_3 molecules. More than one Cu−ammonia complex differing in the number of ammonia ligands has been observed in molecular sieves. Among them a square-planar $Cu^{II}(ND_3)_4$ complex is the most common and is observed in CuH−Y, CuH−SAPO-18, and CuH−SAPO-11.[18,23,27] In CuH−SAPO-5, CuH−SAPO-34, and CuH−SAPO-37 three ammonia molecules are found to coordinate with the Cu ions after adsorption of ammonia.[22,28] However, the observation of two different $Cu^{II}(ND_3)_n$ complexes with the same structure is not observed in other SAPO materials.

Adsorbed C_2D_4 on CuH−SAPO-35 also shows two Cu(II) species J and K. Previously studied Cu-exchanged SAPO materials generally show axially symmetric ESR spectra after ethylene adsorption.[28] Recently we observed a $Cu^{II}C_2D_4$ complex in SAPO-17 with rhombic anisotropy.[20]

Unlike the case of ethylene and ammonia, only one Cu(II) species I is observed after methanol adsorption. Due to its larger kinetic size methanol cannot enter into a hexagonal prism. However, because of its highly polar nature, methanol can pull Cu(II) ions from a hexagonal prism into a levyne cage where they can form complexes. ^{2}D ESEM shows only one CD_3OH molecule directly coordinated to Cu(II). A possible geometry is a distorted tetrahedral complex with Cu(II) coordination to one oxygen of CD_3OH and three oxygens from the framework.

The number of methanols coordinating with Cu(II) varies from structure to structure. A $Cu^{II}(CD_3OH)_2$ complex occurs in Cu-exchanged SAPO-5 and SAPO-11 materials.[23] Similar to SAPO-35, when methanol is adsorbed on CuNa-A and CuK-A, only one molecule coordinates with Cu(II).[29] On the other hand, in materials such as CuNa−X and CuK−X, no direct coordination between Cu(II) and methanol is observed.[30] In dehydrated X zeolites, Cu(II) ions are in a hexagonal prism site due to its high negative charge. The electrostatic interaction between Cu(II) and methanol is not sufficient to pull Cu(II) ions out of a hexagonal prism into a supercage. On the other hand, in the less highly charged CuH−SAPO-37, which is structurally analogous to X zeolite, after methanol adsorption Cu(II) coordinates to three molecules of methanol and is located in a supercage.[28] Also, in SAPO-17, two methanol molecules directly coordinate with Cu(II) ions in a large eronite cage.[20] The levyne cage in SAPO-35 is smaller than the erionite cage in SAPO-17. The various SAPO materials differ mainly in their structure and not in their local charge. Thus, this study shows that the geometry of the specific structure type considerably influences the location and adsorbate coordination of transition-metal ions exchanged into these materials.

Conclusions

Small-pore silicoaluminophosphate molecular sieve SAPO-35 has been synthesized using hexamethyleneimine as a template from aqueous and fluoride media. The main factors affecting crystallinity and phase purity of SAPO-35 are the silica and template concentrations in the gel and the aging time of the gel. Using hexamethyleneimine in aqueous medium SAPO-35 crystallizes in rhombic morphology with highly uniform crystals about 1 μm across. Detailed characterization of SAPO-35 by various physicochemical methods points toward a high level of silicon substitution for framework phosphorus which generates large Bronsted acidity. Two crystallographically distinct framework tetrahedral sites in SAPO-35 are shown by MAS NMR studies. The location of Cu(II) ions exchanged into hydrated H−SAPO-35 is inside a levyne cage as indicated by ^{31}P ESEM data. Dehydration reduces most of the Cu(II) to Cu(I).

(24) Herman, R. G.; Flentge, D. R. *J. Phys. Chem.* **1978**, *82*, 720.
(25) Kevan L: Narayana, M. In *Intrazeolite Chemistry*; Stuckey, G. D., Dwyer, F. G., Eds.; ACS Symp. Ser. Vol. 218; American Chemical Society: Washington, D. C., 1983; pp 283−299.
(26) Zamadics, M.; Chen, X.; Kevan L. *J. Phys. Chem.* **1992**, *96*, 2652.
(27) Wasowicz, T.; Kim, S. J.; Hong, S. B.; Kevan, L. *J. Phys. Chem.* **1996**, *100*, 15954.
(28) Zamadics, M.; Kevan, L. *J. Phys. Chem.* **1993**, *97*, 10102.
(29) Ichikawa, T.; Kevan, L. *J. Am. Chem. Soc.* **1981**, *103*, 5355.
(30) Ichikawa, T.; Kevan, L. *J. Am. Chem. Soc.* **1983**, *105*, 402.

However, treatment with O_2 at higher temperature oxidizes most of the Cu(I) back to Cu(II). Migration of some Cu(II) ions from a levyne cage to a hexagonal prism is also observed during O_2 treatment at high temperature. Adsorption of D_2O on activated CuH−SAPO-35 forms a Cu(II)−aquo complex with axially symmetric ESR parameters ($g_{||} = 2.387$ and $A_{||} = 0.0151$ cm^{-1}). The complex is suggested to be $Cu^{II}(D_2O)_3$ based on ^2D ESEM data. Adsorption of ND_3 on activated CuH−SAPO-35 produces two $Cu^{II}(ND_3)_n$ complexes with axially symmetric ESR parameters. When CD_3OH is adsorbed on activated CuH−SAPO-35, $Cu^{II}(CD_3OH)_1$ is formed based on ^2D ESEM data. Adsorption of C_2D_4 on activated CuH−SAPO-35 gives two $Cu^{II}(C_2D_4)_n$ complexes based on ESR measurements.

Acknowledgment. This research was supported by the National Science Foundation and the Robert A. Welch Foundation. M.H. thanks Deutsche Forschungsgemeinschaft (DFG) for a research fellowship.

CM9707521